

## MIT Open Access Articles

*Model and laboratory study of dispersion  
in flows with submerged vegetation*

The MIT Faculty has made this article openly available. **Please share**  
how this access benefits you. Your story matters.

**Citation:** Murphy, E., M. Ghisalberti, and H. Nepf. "Model and laboratory study of dispersion in flows with submerged vegetation." *Water Resources Research* 43.5 (2007): p. 1-12. ©2007 American Geophysical Union

**As Published:** <http://dx.doi.org/10.1029/2006WR005229>

**Publisher:** American Geophysical Union

**Persistent URL:** <http://hdl.handle.net/1721.1/68011>

**Version:** Final published version: final published article, as it appeared in a journal, conference proceedings, or other formally published context

**Terms of Use:** Article is made available in accordance with the publisher's policy and may be subject to US copyright law. Please refer to the publisher's site for terms of use.



## Model and laboratory study of dispersion in flows with submerged vegetation

E. Murphy,<sup>1</sup> M. Ghisalberti,<sup>2</sup> and H. Nepf<sup>1</sup>

Received 5 June 2006; revised 17 January 2007; accepted 19 February 2007; published 25 May 2007.

[1] Vegetation is ubiquitous in rivers, estuaries, and wetlands, strongly influencing water conveyance and mass transport. The plant canopy affects mean and turbulent flow structure, and thus both advection and dispersion. Accurate prediction for the transport of nutrients, microbes, dissolved oxygen and other scalars depends on our ability to quantify the impact of vegetation. In this paper, we focus on longitudinal dispersion, which traditionally has been modeled in vegetated channels by drawing analogy to rough boundary layers. This approach is inappropriate in many cases, as the vegetation provides a significant dead zone, which may trap scalars and augment dispersion. The dead zone process is not captured in the rough boundary model. This paper describes a new model for longitudinal dispersion in channels with submerged vegetation, and it validates the model with experimental observations.

**Citation:** Murphy, E., M. Ghisalberti, and H. Nepf (2007), Model and laboratory study of dispersion in flows with submerged vegetation, *Water Resour. Res.*, 43, W05438, doi:10.1029/2006WR005229.

### 1. Introduction

[2] Traditionally, vegetation has been removed from waterways to improve conveyance [Lopez and Garcia, 2001]. However, it is now known that vegetation directly improves the quality of coastal and inland waters through nutrient uptake and oxygen production [Kadlec and Knight, 1996]. For example, aquatic macrophytes sequester nitrogen and phosphorus, so that some researchers now advocate widespread planting in waterways [Mars et al., 1999]. The fate and transport of contaminants is also affected by the presence of vegetation, which dramatically alters the flow dynamics [Ghisalberti and Nepf, 2002]. Reduced velocity due to canopy drag promotes the deposition of sediment grains, which can aid in the removal of absorbed contaminants [Leonard and Luther, 1995; Leonard and Reed, 2002; Lopez and Garcia, 1998; Palmer et al., 2004]. The baffling effect of vegetation suppresses turbulence [Nepf, 1999], which influences the growth and distribution of organisms such as phytoplankton [Leland, 2003]. Finally, residence time within the canopy is also strongly affected by vegetation density [Oldham and Sturman, 2001; Schultz et al., 2002; Nepf et al., 2007].

[3] In aquatic systems, the primary impact of submerged vegetation is an increase in flow resistance and subsequent reduction in conveyance capacity [see, e.g., Kouwen et al., 1969; Stephan and Gutknecht, 2002; Stone and Shen, 2002, and references therein]. More recent work has shown in greater detail how submerged vegetation alters both the mean and turbulent structure of the flow [Ikeda and

Kanazawa, 1996; Ghisalberti and Nepf, 2004; Poggi et al., 2004]. In particular, the velocity profile is far from logarithmic over the full depth, so that traditional treatment of longitudinal dispersion in open channels cannot be directly applied to vegetated ones. While dispersion in flows with emergent vegetation has been studied [Nepf et al., 1997a; White and Nepf, 2003; Lightbody and Nepf, 2006], the effect of submerged vegetation on dispersion has not been fully investigated.

[4] The coefficient of longitudinal dispersion ( $K_x$ ) describes the growth rate of the longitudinal variance ( $\sigma_x^2$ ) of a tracer cloud, according to

$$K_x = \frac{1}{2} \frac{d\sigma_x^2}{dt} \quad (1)$$

After a sufficient time since release,  $\sigma_x^2$  increases linearly with time and  $K_x$  reaches a constant value, indicating that the Fickian limit has been reached. In wide channels, dispersion is dominated by vertical shear, and, in the Fickian limit,  $K_x$  is given by

$$K_x = -\frac{1}{H} \int_0^H u'' \int_0^z \frac{1}{D_z} \int_0^z u'' dz dz \quad (2)$$

[see Fischer et al., 1979, pp. 91]. Here  $z$  is the vertical coordinate with  $z = 0$  at the bed,  $H$  is the flow depth,  $u''$  is the local deviation from the depth-averaged velocity  $\langle U \rangle$ , and  $D_z$  is the vertical diffusivity. In a wide, straight channel with a logarithmic velocity profile, equation (2) reduces to  $K_x = 5.93 u_{*H} H$  [Elder, 1959]. Here  $u_{*H}$  denotes the friction velocity,

$$u_{*H} = \sqrt{gSH} \quad (3)$$

where  $S$  is the potential gradient due to channel-bed slope and/or water-surface slope. Elder's analytical prediction is

<sup>1</sup>Department of Civil and Environmental Engineering, Massachusetts Institute of Technology, Cambridge, Massachusetts, USA.

<sup>2</sup>School of Environmental Systems Engineering, University of Western Australia, Crawley, Western Australia, Australia.

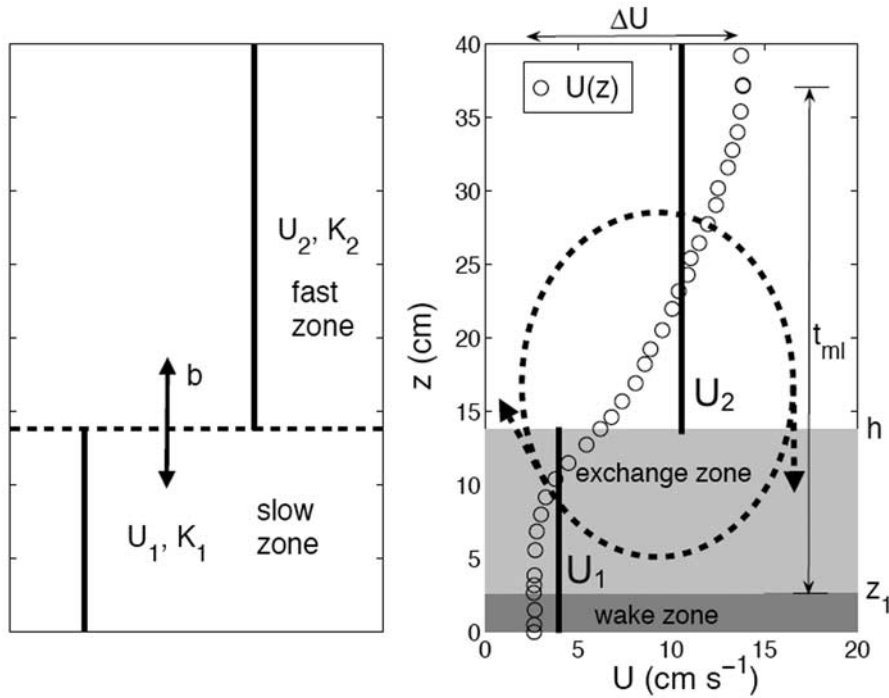


**Figure 1.** (a) Two-zone model with top of the canopy at  $z = h$ . The channel depth,  $H$ , is divided into a fast zone of thickness  $(H - h)$  and a slow zone within the canopy ( $0 < z < h$ ). (b) The vertical profile of velocity,  $U$ , for run H (Table 1). The canopy is separated into an upper exchange zone ( $z_1 < z < h$ ) with rapid vertical exchange and a lower wake zone ( $0 < z < z_1$ ) with greatly reduced turbulent velocity and length scales.

comparable to dispersion coefficients observed in wide ( $w_c/H \geq 10$ , where  $w_c$  is the channel width), straight, rough-bottomed laboratory channels [Fischer, 1973]. However, these conditions do not hold in all aquatic systems. Lateral nonuniformity in rivers, such as bends and dead zones, can result in significant lateral shear that dramatically increases dispersion [Day, 1975; Nordin and Troutman, 1980; Davis *et al.*, 2000]. Similarly, the drag imparted by submerged vegetation generates a velocity profile that differs from a logarithmic boundary layer [Ghisalberti and Nepf, 2005], such that Elder's analysis does not directly apply. In this paper, we use new information on the physics of vegetated flow (described in section 2) to formulate a predictive model for dispersion in vegetated channels, and we validate the model experimentally.

## 2. Two-Zone Model for Vegetated Flows

[5] The diminished fluid velocity in a layer of submerged vegetation makes it distinct from the overflowing water. We therefore propose a two-zone model for vegetated channels with a division at the top of the canopy ( $z = h$ ), as in Figure 1a. A uniform velocity,  $U_1$  and  $U_2$ , is assumed within the lower and upper zone, respectively.  $K_1$  and  $K_2$  are the longitudinal dispersion constants in the lower and upper zones, respectively. Scalar transport between the two layers is characterized by the exchange coefficient,  $b$ , which has dimensions "time<sup>-1</sup>".

[6] This approach is similar to transient storage, or dead zone models, which have been developed to explain the persistently skewed concentration distributions observed in natural channels [Day, 1975; Nordin and Troutman, 1980;

van Masijk and Veling, 2005]. These observations have led to widespread consensus that the characterization of longitudinal dispersion in rivers must explicitly consider the effect of "dead", or "slow" zones [Valentine and Wood, 1977; Chikwendu and Ojiakor, 1985]. Several multilayer models have emerged [e.g., Thacker, 1975; Smith, 1981; Chikwendu and Ojiakor, 1985; Roberts and Strunin, 2004]. The basis for most analyses is the application of coupled advection-dispersion equations in each region of flow. Chikwendu [1986] derived an expression for dispersion in a flow with  $N$  distinct velocity zones. Here we choose two zones ( $N = 2$ ). Then, Chikwendu's equation (3.3) reduces to the following prediction for longitudinal dispersion coefficient at large times.

$$K_x = \frac{\left(\frac{h}{H}\right)^2 \left(\frac{H-h}{H}\right)^2 (U_2 - U_1)^2}{b} + \left(\frac{h}{H}\right) K_1 + \left(\frac{H-h}{H}\right) K_2 \quad (4)$$

$U_1$  and  $U_2$  are the layer-averaged velocity in slow-and fast-zone, respectively, as shown in Figure 1. Equation (4) highlights three distinct processes that contribute to dispersion in channels containing submerged vegetation. The first term in equation (4) represents dispersion arising from the inefficient exchange between the fast zone ( $h < z < H$ ) and the slow zone ( $0 < z < h$ ). In other words, scalar trapped in the canopy (slow-zone) is held up relative to scalar in the overflow (fast-zone), increasing the spread of mass in the longitudinal direction. The second and third terms in equation (4) represent the dispersion in the canopy and in the overflow, respectively.

[7] As first presented by *Raupach et al.* [1996], the flow structure near the top of a submerged canopy resembles a mixing layer, rather than a boundary layer (Figure 1b). A mixing layer is a confined region of shear (of size  $t_{\text{ml}}$ ) that separates two regions of approximately constant velocity. The velocity difference across the layer is denoted by  $\Delta U$ . The mixing layer is characterized by a street of coherent Kelvin-Helmholtz (K-H) vortices that dominate vertical transport between the canopy and overflowing layer [*Ikeda and Kanazawa*, 1996; *Ghisalberti and Nepf*, 2005]. These structures reach a fixed scale and a fixed penetration into the canopy at a short distance from the canopy's leading edge (*Ghisalberti and Nepf*, 2004). The penetration distance,  $(h - z_1)$ , Figure 1), segregates the canopy into an upper layer with rapid transport and a lower layer with slow transport [*Nepf and Vivoni*, 2000]. The upper layer, called the exchange zone, spans  $z_1 < z < h$ . Vertical transport in this region is dominated by the coherent structures. The lower layer, called the wake zone, spans  $0 < z < z_1$ . Vertical transport in this region is controlled by stem-wake turbulence, which has significantly smaller length-and velocity-scales than the K-H vortices. Consequently, vertical transport in the wake zone is typically an order of magnitude slower than that in the exchange zone [*Ghisalberti and Nepf*, 2005].

[8] *White et al.* [2003] showed that the vortex penetration distance  $(h - z_1)$  is inversely proportional to the drag coefficient ( $C_D$ ),

$$(h - z_1) \approx 0.2(C_D a)^{-1}, \quad (5)$$

where  $a$  is the projected frontal area of the vegetation per unit volume, which can be related to the leaf area index (LAI) [*Nepf and Vivoni*, 2000, and references therein]. The solid volume fraction within the canopy is then  $ad$ , where  $d$  is the mean diameter of the vegetation.

[9] The exchange coefficient,  $b$ , which appears in the first term of equation (4), is set by the time-scale for transport across both layers,  $T$ . We assume that the time-scale for transport across the upper, open layer is negligible (reasonable for small values of  $H/h$ ), so we can approximate

$$b^{-1} \approx T = \frac{z_1^2}{D_w} + \frac{(h - z_1)}{k} \quad (6)$$

The first term on the right of equation (6) represents the time for turbulent-diffusive transport across the wake zone. In the second term  $k$  ( $\text{cm s}^{-1}$ ) characterizes the vortex-driven flushing of the exchange zone, as described by *Ghisalberti and Nepf* [2005]. Section 2.1 considers the regime where K-H vortices dominate exchange between the layers, such that the first term is negligible. Section 2.2 examines the opposite case, when exchange is limited by turbulent diffusion in the wake zone.

[10] Next, consider the third term in equation (4) in which  $K_2$  represents the longitudinal dispersion in the fast zone due to velocity shear in this region. Above the canopy, the velocity profile reverts to a logarithmic profile for  $z > h$  [*Kouwen et al.*, 1969; *Nepf and Vivoni*, 2000; *Carollo et al.*, 2002]. Thus, Elder's expression should hold in the region  $h < z < H$ , with coefficient  $\gamma = 5.9$ .

$$K_2 = u_*(H - h). \quad (7)$$

For this region the equivalent bed stress is  $\rho u_*^2 = -\overline{\rho u'w'}_{z=h}$ , with

$$u_* = \sqrt{gS(H - h)}. \quad (8)$$

We note again for emphasis that this characterization of  $K_2$  only reflects contributions from vertical shear. It may underestimate conditions in which lateral shear also makes a significant contribution. For such cases a larger value of  $\gamma$  may be appropriate. Finally, in the limit  $H/h \gg 1$ , the combination of equations (4), (7), and (8) gives  $K_x = 5.9 u_{*H} H$ , consistent with boundary layer theory. Similarly, in the limit of emergent vegetation ( $H/h \rightarrow 1$ ),  $K_x = K_1$ .

## 2.1. Vortex-Driven Exchange

[11] In sparse canopies  $z_1/h \ll 1$  and exchange is driven by the K-H vortices that penetrate deep into the canopy. Experiments by *Ghisalberti and Nepf* [2005] show that vortex-driven exchange may be described by an exchange velocity  $k = \Delta U/40$ , so that in this limit of behavior

$$b = \frac{\Delta U}{40h}. \quad (9)$$

Furthermore, we assume that the difference in layer velocities,  $U_2 - U_1$ , is a constant fraction,  $\beta_1$ , of the total velocity difference,  $\Delta U$ , i.e.

$$(U_2 - U_1) = \beta_1 \Delta U \quad (10)$$

[12] Previous studies suggest that  $\overline{u'w'} \sim (\Delta U)^2$  [*Ghisalberti and Nepf*, 2005], so that it is reasonable to assume  $\beta_2 = \Delta U/u_*$  is approximately constant. The assumptions of constant  $\beta_1$  and  $\beta_2$  are verified for our canopy in section 5. The exchange term in equation (4) is then simplified by substitution of equations (9), (10), and  $\Delta U = \beta_2 u_*$ . Based on the dispersion observed in emergent canopies [*White and Nepf*, 2003; *Nepf et al.*, 1997a], the term in equation (4) containing  $K_1$  is expected to be small compared to the other terms, and is neglected for simplicity. Finally, equation (7) is used for  $K_2$ ,

$$K_x = 40\beta_1^2\beta_2 \left(\frac{h}{H}\right)^2 \left(\frac{H-h}{H}\right)^2 hu_* + \gamma \frac{(H-h)^2}{H} u_* \quad (11)$$

For convenience, we combine the constants  $40\beta_1^2\beta_2 = \beta$  and divide through by  $u_{*H}H$ , obtaining the following nondimensional coefficient of longitudinal dispersion.

$$\frac{K_x}{u_{*H}H} = \beta \left(\frac{h}{H}\right)^3 \left(\frac{H-h}{H}\right)^{5/2} + \gamma \left(\frac{H-h}{H}\right)^{5/2} \quad (12)$$

## 2.2. Diffusion-Limited Exchange

[13] In dense canopies,  $z_1/h \approx 1$  and vortex penetration is limited. With these conditions the in-canopy diffusion controls exchange between the canopy and overflow. When  $z_1 = h$ , equation (6) reduces to

$$b \approx \frac{D_w}{h^2} \quad (13)$$

We assume the wake-zone diffusivity,  $D_w$ , approximates the value observed in emergent canopies, and use the

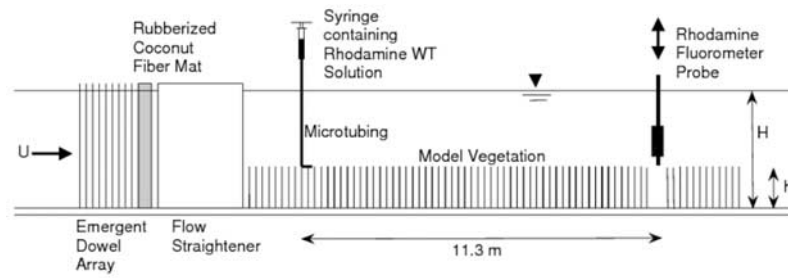


**Figure 2a.** Experimental setup (not to scale).

relationship observed in field canopies [Lightbody and Nepf, 2006],

$$D_w = 0.17U_1d \quad (14)$$

Substituting equations (13) and (14) into equation (4) and applying similar simplifications to those in section 2.1,

$$\frac{K_x}{u_{*H}H} = \frac{1}{0.17} \left( \frac{U_2 - U_1}{u_{*H}} \right)^2 \left( \frac{h}{H} \right)^3 \left( \frac{H-h}{H} \right)^2 \left( \frac{h}{d} \right) \frac{u_{*H}}{U_1} + 5.9 \left( \frac{H-h}{H} \right)^{5/2} \quad (15)$$

Because vegetative drag is the dominant resistance for  $ad \geq 0.01$  [Nepf, 1999], the depth-averaged force balance for steady conditions can be written

$$\rho gSH \approx \frac{1}{2} \rho C_D ah U_1^2. \quad (16)$$

Then, using equation (3) to simplify the left-hand side of equation (16),

$$\frac{u_{*H}}{U_1} = \left( \frac{C_D ah}{2} \right)^{1/2} \quad (17)$$

Substitution of equation (17) into equation (15) yields

$$\frac{K_x}{u_{*H}H} = \zeta \left( \frac{h}{H} \right)^3 \left( \frac{H-h}{H} \right)^2 \left( \frac{h}{d} \right) (C_D ah)^{1/2} + 5.9 \left( \frac{H-h}{H} \right)^{5/2} \quad (18)$$

The coefficient  $\zeta = 4.2[(U_2 - U_1)/u_{*H}]^2$  will be evaluated with experimental observations.

### 3. Experimental Methods

[14] Experiments were conducted in a 24-m-long  $\times$  38-cm-wide  $\times$  58-cm-deep, glass-walled recirculating flume (Figures 2a and 2b). The flow rate was controlled

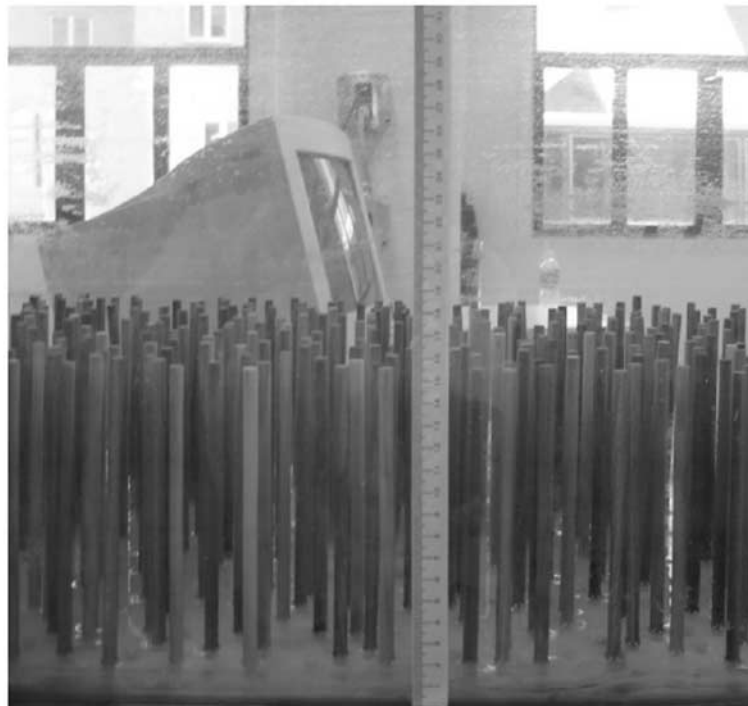


**Figure 2b.** Model canopy.

by a Weinman 3G-30P14 pump, with a capacity of 600 to 15,000 cm<sup>3</sup>/s. A Signet flow gauge, with  $\pm 200$  cm<sup>3</sup>/s accuracy, provided flow rate. A number of measures were taken to ensure smooth inlet conditions. A dense, 0.5-m-long array of emergent wooden dowels and mats of rubberized coconut fiber were used to break up inlet turbulence. A 1-m section of honeycomb eliminated swirl, providing unidirectional flow. The flume had zero bed-slope, so that the potential gradient was associated with water-surface gradient only. However, the surface gradient was too small to measure using surface displacement gages. Therefore  $S$  was estimated from the Reynolds' stress profiles in the upper water region, as described by *Ghisalberti and Nepf* [2004].

[15] The model plant canopy consisted of maple cylinders (diameter,  $d = 6$  mm), inserted in a random configuration into perforated Plexiglas boards, which covered the entire length of the flume. The canopy density was varied between  $ad = 0.015$  and  $ad = 0.048$ , within a range representative of field conditions, as cited by *Ghisalberti and Nepf* [2004]. Two canopy heights were employed, 7 and 14 cm. Velocity profiles for runs A through I were measured by acoustic Doppler velocimeters, as reported in *Ghisalberti and Nepf* [2004]. For the remaining runs, velocity measurements were taken by a two-dimensional (2-D) laser Doppler velocimeter (LDV). A 300-mW blue-green argon-ion laser was used in conjunction with a Dantec 58N40 flow velocity analyzer (FVA) unit. Vertical profiles were taken at midwidth in the flume and consisted of 5-min records taken at vertical intervals between 0.5 and 2 cm, depending on the precision required. All measurements were taken sufficiently far downstream of the canopy's leading edge that the flow was fully developed (i.e.,  $\partial/\partial x = 0$ ). Velocity records were decomposed into a temporal-average and turbulent fluctuations in the  $x$ -(longitudinal) and  $z$ -(vertical) directions, respectively

$$u(t) = U + u'(t) \quad (19)$$

$$w(t) = W + w'(t) \quad (20)$$

The LDV probe was aligned so that  $W = 0$ .

[16] Twenty-four flow scenarios were investigated, with different discharge,  $Q$ , canopy density,  $ad$ , and relative submergence,  $H/h$ . The Reynolds number ( $Re_H = \langle U \rangle H/\nu$ ,  $\langle \rangle$  denotes a depth average) was between 3000 and 41,000, consistent with values observed in natural channels.

[17] Tracer experiments were conducted by releasing a small pulse of fluorescent dye at the top of the canopy, and 6 m downstream of the leading edge. This longitudinal position was observed to be well within the region of fully developed flow, determined by a sequence of velocity profiles. The tracer consisted of a mixture of Rhodamine WT dye and isopropyl alcohol, with the latter added to render the solute neutrally buoyant in the flume. The dye was injected manually with a 60-ml syringe, through micro-tubing (1 mm I.D.) glued to the top of a dowel at midwidth and oriented parallel to the flow. Care was taken to match the injection speed with local water speed, to limit near-field mixing. The duration of the injection was minimized, to mimic a pulse, and subsequent leakage of tracer into the flow was eliminated by rawal of the syringe.

[18] The depth-averaged concentration of dye was measured as a function of time, at a location 11.3 m downstream of the injection point. This was done using a Rhodamine fluorometer, with a sampling rate of 8 Hz. In all cases, the traveltime of the tracer cloud from its point of injection to the probe was much greater than the time taken to introduce the dye, confirming that the injection approximated an instantaneous release. For most experiments the fluorometer was mounted at midwidth in the flume on a pulley system that allowed smooth, precise maneuvering in the vertical plane. As the tracer cloud advected past, the fluorometer was repeatedly raised and dropped at timed intervals, so that the entire water depth was sampled. The vertical traverse time was sufficiently short compared to the timescale of tracer passage, that the vertical profile could be considered an instantaneous snapshot and was used to estimate the instantaneous depth-averaged concentration. Experimental runs were terminated when tracer mass in the leading edge of the cloud had recirculated around the flume. Each condition was repeated five times. For several cases the fluorometer was positioned at three different lateral locations for the same flow condition. The difference in dispersion coefficient obtained at each location was within the uncertainty of the method, demonstrating that a single measure at midwidth was sufficient.

[19] The temporal variance,  $\sigma_t^2$ , of the measured concentration-time distributions was calculated using the method of moments [*Aris*, 1956],

$$\sigma_t^2 = \frac{M_2}{M_0} - \left( \frac{M_1}{M_0} \right)^2 \quad (21)$$

$M_i$  denotes the  $i$ th temporal moment, obtained from the concentration record,  $C(t)$ , by

$$M_i = \int_{-\infty}^{\infty} t^i C(t) dt \quad (22)$$

The velocity,  $U_c$ , of the center of mass is

$$U_c = X/\mu \quad (23)$$

where  $X$  is the distance between the point of injection and the fluorometer (11.3 m), and  $\mu$  is the arrival time of the center of mass, which is obtained from

$$\mu = M_1/M_0 \quad (24)$$

Combining a minimum of five realizations of each experiment yielded ensemble-averaged values of  $U_c$  and  $\sigma_t$ . The frozen cloud approximation [*Fischer et al.*, 1979, p. 137] was applied; that is, the tracer mass was assumed not to disperse appreciably, as it passed the fluorometer. The spatial variance was then inferred from the Lagrangian velocity of the tracer,

$$\sigma_x^2 = \sigma_t^2 U_c^2 \quad (25)$$

and longitudinal dispersion coefficients were estimated as  $K_x = \sigma_x^2/2\mu$ , an approximation of equation (1). Here it is

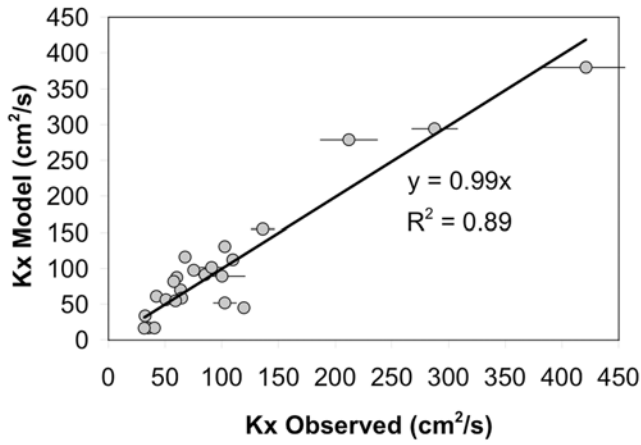


**Figure 3.** Modeled  $K_x$  versus observed  $K_x = \sigma_x^2/2\mu$ . Horizontal bars indicate the standard error of multiple realizations,  $\varepsilon_{K_x}$  in Table 2. Correlation between the modeled and laboratory data is highly significant ( $R^2 = 0.89$ ,  $n = 24$ ).

assumed that  $X$  is sufficiently large for the solute to reach a Fickian dispersive regime. *Fischer* [1973] proposed that this regime is achieved beyond the time,

$$t_f = 0.4 \frac{H^2}{\langle D_z \rangle} \quad (26)$$

Uncertainty in the approximation,  $K_x = \sigma_x^2/2\mu$  was investigated using a two-dimensional ( $x$  and  $z$ ) particle-tracking model for open channel flow, developed by B. L. White at M.I.T., in the Netlogo programming environment [Wilensky, 1999]. The model was modified to represent the specific hydrodynamic conditions of each experimental run. Full model details are given by *Murphy* [2006]. In the random walk particle-tracking (RWPT) model, particles are advected with the time-mean velocity,  $U(z)$ , and vertical diffusion is simulated by random jumps in the vertical. Longitudinal diffusion is neglected, as it is small compared to longitudinal dispersion. For simplicity, a stepped profile of vertical diffusivity,  $D_z$ , was used in the model. For the wake zone  $z < z_1$ ,  $D_z = D_w$  obtained from Figure 7 by *Nepf et al.* [1997b]. For  $z > z_1$ , the diffusivity was assigned a mean value based on the estimated or observed  $D_z$  profile,

$$\langle D_{z,sl} \rangle = \frac{1}{H - z_1} \int_{z_1}^H D_z dz. \quad (27)$$

Experimentally determined  $D_z$  profiles were available from *Ghisalberti and Nepf* [2005] for runs A through I. For the remaining runs diffusivity profiles were computed from measured Reynolds' stress profiles, using  $D_z(z) = \nu_{tz}(z)/S_{ct}$ , where  $\nu_{tz}$  is the turbulent eddy viscosity,

$$\nu_{tz} = -\frac{\overline{u'w'}}{\partial U / \partial z}, \quad (28)$$

and the turbulent Schmidt number,  $S_{ct}$ , was taken to be 0.5 based on previous observ in vegetated shear layers

[*Ghisalberti and Nepf*, 2005]. In the upper water column, where low values of shear made equation (28) unstable, we assume  $D_z = 0.013 \Delta U t_{ml}$  as suggested by *Ghisalberti and Nepf* [2005].

[20] In RWPT models, a discontinuous diffusivity profile can result in artificial particle accumulation in regions of low diffusivity [Thomson et al., 1997; Hoteit et al., 2002; Ross and Sharples, 2004]. A correction was therefore applied, by treating the diffusivity discontinuity interface as a semireflecting boundary [see e.g., Ross and Sharples, 2004]. The approach was deemed appropriate following observations that particles, when introduced as a line source over depth, remained uniformly distributed with time [Thomson et al., 1997].

[21] Ten thousand particles (sufficient to provide statistical convergence) were released at  $z = h$  and tracked for 3000 s, or until  $K_x = 0.5 \sigma_x^2/t$  became constant with time. To validate the model, predictions of dispersion coefficient were made for each of the experimental runs, at the time corresponding to the experimental  $\mu$ . The correlation between the predicted and observed values was highly significant (Figure 3,  $R^2 = 0.89$ ,  $n = 24$ ), suggesting that the model correctly represents the dispersion process.

#### 4. Results and Discussion

[22] Flow parameters for the 24 experiments are listed in Table 1. The first seven rows correspond to runs of the same letter in the work of *Ghisalberti and Nepf* [2004]. Physical constraints of the flume limit the range of  $z_1/h$ , such that  $z_1/h \ll 1$  for most of the experiments. Therefore the discussion of experiments will focus on the vortex-driven exchange model given in equation (12).

[23] The concentration-time distribution for run A5 is shown in Figure 4. Individual realizations are consistent with the average, indicating that the number of repetitions is adequate. A nonzero skewness coefficient (shown in Figure 4) reveals a slight deviation from Gaussian form that agrees with observations in natural channels [Nordin and Troutman, 1980]. The statistics of the temporal concentration distributions are presented in Table 2, along with the dispersion coefficients obtained from the approximation  $K_x = \sigma_x^2/2\mu$ .  $\varepsilon_{K_x}$  is the standard error over multiple realizations. In all cases the Peclet number,  $Pe = U_c X / K_x \gg 1$ , validated the frozen cloud assumption made in section 3 [Levenspiel and Smith, 1957].

[24] Over the full range of  $H/h$   $u_* = \sqrt{gS(H-h)}$  is a consistent estimator for the Reynolds' stress measured at the top of the canopy, with  $u_* / (-\overline{u'w'_h})^{1/2} = 1.1 \pm 0.1$  (Figure 5). In contrast,  $u_{*H} / (-\overline{u'w'_h})^{1/2}$  varies considerably. As expected,  $u_*$  and  $u_{*H}$  converge for  $H/h > 1$ . Furthermore, the ratio  $\beta_2 = \Delta U / u_* = 6.1 \pm 1.1$  (SD) and is not significantly correlated with either  $H/h$  (Figure 6,  $R^2 = 0.05$ ,  $n = 24$ ), or  $C_{Dah}$  (Figure 7,  $R^2 = 0.006$ ,  $n = 24$ ). The parameter  $\beta_1 = (U_2 - U_1) / \Delta U = 0.68 \pm 0.04$  (SD) and has no correlation with  $H/h$  (Table 1,  $R^2 = 0.004$ ,  $n = 24$ ). Given these values we expect  $\beta = 40 \beta_1^2 \beta_2 = 110 \pm 20$ .

[25] The results of the RWPT model simulations suggest that a more stringent criterion than  $t > t_f$  is required when the single-point estimate is used to determine  $K_x$ . As an example, we consider run C1. Both the instantaneous coefficient,  $K_x = 0.5 \partial \sigma_x^2 / \partial t$ , as well as the single-point estimate,  $K_x = \sigma_x^2 / 2t$ , are calculated from the RWPT results

**Table 1.** Summary of Experimental Conditions and Flow Parameters

Run	$Q \times 10^{-2} \text{ cm}^3 \text{ s}^{-1}$	$h, \text{ cm}$	$H, \text{ cm}$	$a, \text{ cm}^{-1}$	$S \times 10^5$	$U_1, \text{ cm s}^{-1}$	$U_2, \text{ cm s}^{-1}$	$\Delta U, \text{ cm s}^{-1}$	$\beta_1$	$h - z_1, \text{ cm}$	$Re_H \times 10^{-4}$
A	48	14.0	46.7	0.025	0.99	1.6	3.7	3.2	0.67	12.7	1.5
C	74	14.0	46.7	0.034	2.50	2.0	5.5	4.9	0.71	10.9	2.1
D	48	14.0	46.7	0.034	1.20	1.4	3.8	3.5	0.67	12.3	1.4
E	143	14.0	46.7	0.040	7.50	4.2	10.6	9.5	0.68	11.6	4.1
G	48	14.0	46.7	0.040	1.30	1.4	3.7	3.3	0.69	10.3	1.4
H	143	14.0	46.7	0.080	10.00	3.3	11.1	11	0.71	11.2	4.1
I	94	14.0	46.7	0.080	3.40	2.1	7.2	7.4	0.69	9.8	2.7
A6	17	7.0	29.8	0.025	0.30	0.6	1.6	1.6	0.64	5.8	0.4
B6	94	7.0	29.8	0.025	8.04	3.3	8.4	7.0	0.73	7.0	2.2
C6	48	7.0	29.8	0.025	2.42	1.7	4.4	3.7	0.70	3.4	1.1
A1	17	7.0	23.6	0.025	1.06	0.7	1.6	1.4	0.68	7.0	0.3
B1	94	7.0	23.6	0.025	11.57	4.3	10.2	9.1	0.65	7.0	2.0
C1	48	7.0	23.6	0.025	4.27	2.2	5.1	4.8	0.61	5.1	1.0
A2	17	7.0	14.0	0.025	1.73	1.3	2.9	2.4	0.67	7.0	0.3
B2	94	7.0	14.0	0.025	48.66	7.8	15.5	11.8	0.65	7.0	1.7
C2	48	7.0	14.0	0.025	30.05	5.0	10.6	7.8	0.72	7.0	1.1
A3	17	7.0	10.5	0.025	12.44	2.5	5.4	5.0	0.59	2.9	0.4
C3	48	7.0	10.5	0.025	66.61	6.9	14.7	11.0	0.71	7.0	1.0
A5	17	7.0	8.8	0.025	28.35	2.8	5.3	3.2	0.77	3.9	0.3
C5	48	7.0	8.8	0.025	134.04	9.9	18.7	12.6	0.70	7.0	1.1
C6D	48	7.0	29.8	0.080	2.03	0.8	4.6	5.3	0.72	7.0	1.1
C2D	48	7.0	14.0	0.080	36.64	3.0	9.3	9.5	0.66	7.0	0.9
A2D	17	7.0	14.0	0.080	4.74	1.0	3.4	3.4	0.70	5.3	0.3
A3D	17	7.0	10.5	0.080	23.19	2.0	5.2	4.6	0.71	5.4	0.3

and compared in Figure 8. As expected, the instantaneous  $K_x$  reaches its asymptotic limit just after the Fickian time-scale,  $t_f$ , and remains constant, with minor fluctuation, after that. In contrast, the point-approximation does not reach the Fickian  $K_x$  value until  $t \approx t_{10\%}$ ; i.e., the approximation of equation (1) by  $\sigma_x^2/2\mu$  will underestimate  $K_x$  until some time after the onset of a Fickian regime. We propose  $t_{10\%}$ , the time when the point approximation of  $K_x$  becomes accurate to within 10% (see Figure 8), as an appropriate value. On the basis of the range of conditions considered here,  $t_{10\%} = 2.9 t_f$  (Figure 9,  $R^2 = 0.88$ ,  $n = 24$ ). Because  $\mu < t_{10\%}$  for many of the experimental runs (Table 2), it is likely that  $K_x$  values obtained from  $\sigma_x^2/2\mu$  are underestimates of the desired Fickian value. In cases for which  $\mu < t_{10\%}$ , the RWPT results are used to adjust the measured dispersion coefficient,  $K_{x,\text{adj}}$  in Table 2. For example, in run C1 (Figure 8), at  $t = \mu$  the RWPT model indicates  $\sigma_x^2/2\mu = 69 \text{ cm}^2 \text{ s}^{-1}$ , which is close to observed value  $K_{x,o} = 64 \pm 4 \text{ cm}^2 \text{ s}^{-1}$ , but falls short of the asymptotic Fickian value. For this run, the dispersion coefficient is adjusted upward to  $K_x = 75 \text{ cm}^2 \text{ s}^{-1}$ , in accordance to the RWPT results.

[26] Figure 10 shows the raw experimental data (diamonds) and the adjusted data (circles), ensemble-averaged for each value of  $H/h$ . Model equation (12) with coefficients  $\beta = 110$  and  $\gamma = 5.9$  is shown as a gray line. A least squares best fit of equation (12) to the adjusted data yields a value of  $\beta = 140 \pm 20$  and  $\gamma = 6.9 \pm 0.6$ . This curve is shown as a solid black line in Figure 10. The fitted value for  $\beta$  agrees within uncertainty with the value predicted from velocity data ( $\beta = 110 \pm 20$ ). However, the coefficient for the upper-layer dispersion,  $\gamma$ , slightly exceeds the value for logarithmic boundary layers ( $\gamma = 5.9$ ), suggesting that the analogy between overcanopy flow and boundary layer flow is not exact. Future models should consider the velocity structure in this region more closely. The dashed and dash-dot lines in Figure 10

represent the contributions of the exchange-zone and fast-zone-shear dispersion terms, respectively, for  $\beta = 140$  and  $\gamma = 6.9$ . For  $H/h < 2.5$  inefficient exchange between layers is the primary mechanism for dispersion. Realistically,  $K_x$  will not go to zero at  $H/h = 1$  but will assume the small finite value of  $K_1$  in the limit of emergent vegetation. As  $H/h$  increases, shear dispersion in the fast zone grows in importance and becomes the dominant at  $H/h \approx 2.7$ .

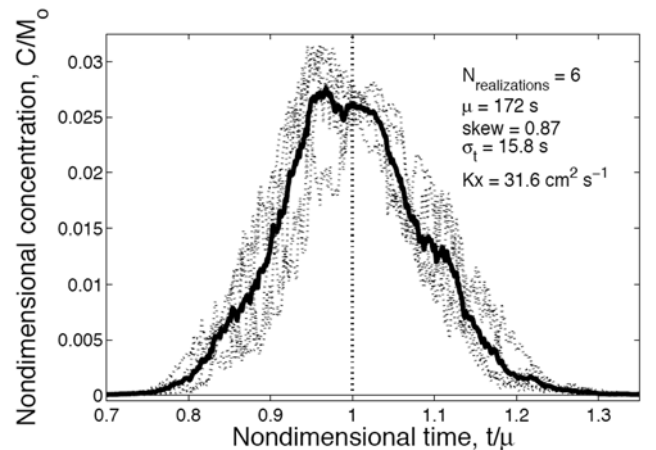


**Figure 4.** Concentration-time curves for run A5. The ensemble average (solid line) is superimposed on the individual realizations (dotted curves). The time and concentration axes are normalized by the mean arrival time,  $\mu$ , and the total recovered solute mass,  $M_0$ , respectively. Normalization eliminates, so far as is possible, nonuniformities across realizations caused by slight differences in the masses of tracer injected [White and Nepf, 2003].



**Table 2.** Temporal Moment Analysis of Concentration Distribution

Run	$\mu$ , s	$\sigma_t$ , s	$Pe$	$K_x$ , $\text{cm}^2 \text{s}^{-1}$	$\varepsilon_{K_x}$ , $\text{cm}^2 \text{s}^{-1}$	$\frac{\mu}{t_{10\%}}$ <sup>a</sup>	$K_{x,adj}$ <sup>a</sup> , $\text{cm}^2 \text{s}^{-1}$
A	390	89.1	39	85	10	0.3	130
C	252	58.4	37	140	10	0.3	210
D	356	80.3	40	90	10	0.2	150
E	137	34.1	32	290	20	0.4	440
G	382	81	45	75	5	0.2	120
H	123	35.2	25	420	30	0.2	690
I	192	48.6	31	210	25	0.2	380
A6	729	140	55	32	2	0.4	43
B6	141	21.1	89	100	10	1.6	110
C6	252	38.9	84	60	3	0.2	110
A1	567	100	65	35	3	0.5	44
B1	96.8	13	110	120	5	1.4	130
C1	192	26.6	104	64	4	0.7	75
A2	332	48.3	95	41	5	0.9	46
B2	60.7	5.9	210	100	20	0.7	110
C2	117	12.1	189	58	1	0.7	66
A3	234	29.2	129	42	3	0.4	60
C3	89.4	8.7	211	68	1	1	75
A5	172	15.8	235	32	1	0.6	41
C5	70.3	5.9	281	65	4	1.3	70
C6D	289	62.2	43	103	5	0.5	130
C2D	128	19	91	110	5	1	120
A2D	326	52.3	77	51	4	0.5	61
A3D	231	33.8	93	60	1	1.1	65

<sup>a</sup>Based on results of the RWPT model.

[27] It is interesting to note that  $K_x$  also has a significant correlation with  $u_{*H}H$ , the parameterization suggested by Elder (Figure 11,  $R^2 = 0.83$ ,  $n = 24$ ). On the basis of this we suggest a second, simpler model,  $K_x = (5.0 \pm 0.7) u_{*H}H$ . The two models are compared in Figure 12. Model equation (12) has better agreement with experimental values ( $R^2 = 0.81$ ,  $n = 24$ ) than the model based on correlation ( $R^2 = 0.72$ ,  $n = 24$ ). In particular, equation (12) does better at lower

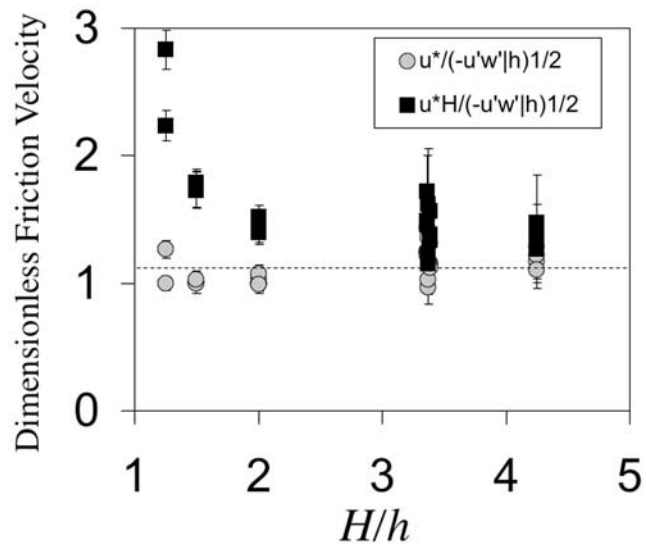


**Figure 5.** Friction velocities  $u_* = \sqrt{gS(H - h)}$  (circles) and  $u_{*H} = \sqrt{gSH}$  (squares), each normalized by the square root of the Reynolds stress at the top of the canopy,  $\sqrt{-u'w'_h}$ . Vertical bars represent uncertainty. Dashed line indicates mean across all  $u_*/\sqrt{-u'w'_h} = 1.1 \pm 0.1$ .

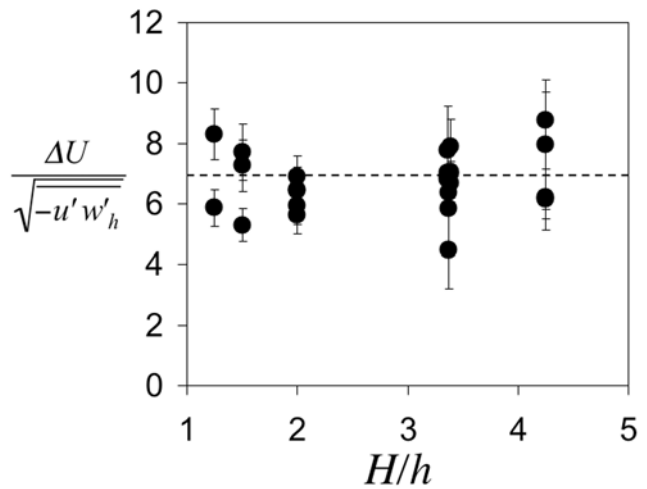


**Figure 6.** The velocity difference  $\Delta U$  normalized by  $u_*$  over the range of  $H/h$ . Vertical bars indicate uncertainty. The dashed line indicates the mean value,  $\Delta U/u_* = 6$ , across all cases.

values of  $K_x$ , which are associated with the lower values of  $H/h$ . This is consistent with Figure 10, which shows that  $K_x/u_{*H}H$  is approximately constant only for  $H/h > 2$ , but drops off below this in the region dominated by inefficient exchange. The correlation model fails to follow this trend. One concludes that for shallow submergence ( $H/h \leq 2$ ) model equation (12) is required in order to properly capture the contribution from inefficient exchange. But, for relative submergence  $H/h > 2$ , the simpler correlation model is sufficient.

[28] Finally, the value  $K_x/u_{*H}H$  observed for  $H/h < 5$  is smaller than that predicted for an unvegetated channel of the same depth, i.e., for an unobstructed logarithmic boundary layer. Let us explore why. In these experiments,

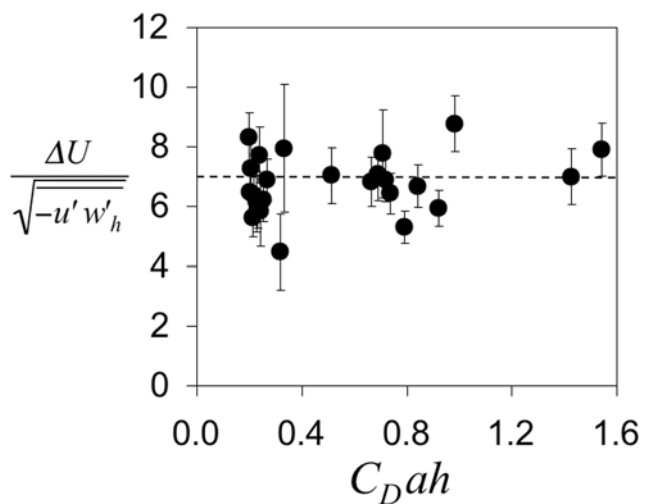


**Figure 7.** Velocity difference  $\Delta U$  normalized by  $u_*$ . Vertical bars indicate uncertainty. The dashed line indicates the mean value,  $\Delta U/u_* = 6$ , across all cases.  $C_D$  was estimated based on reported values for isolated, long-aspect ratio cylinders [see e.g., White, 1974, p. 210].

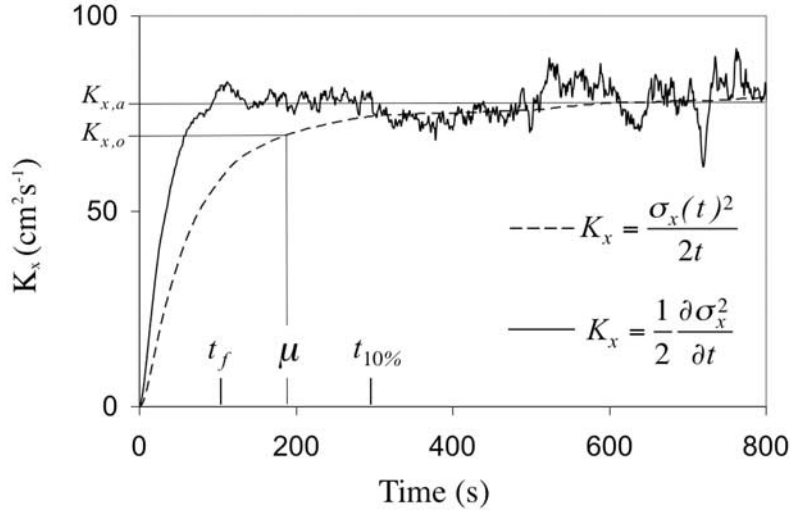


**Figure 8.** RWPT simulation for run C1. The estimator  $K_x = \sigma_x^2/2t$  is shown as a dashed line, and the instantaneous  $K_x = 0.5\partial\sigma_x^2/\partial t$  is shown as a solid line. At  $t = \mu$ , the approximation  $K_x = \sigma_x^2/2\mu = 69 \text{ cm}^2 \text{ s}^{-1}$  is close to observed value  $K_{x,o} = 64 \pm 4 \text{ cm}^2 \text{ s}^{-1}$ . However, both fall short of the asymptotic value  $K_{x,a}$ . Although the dispersion is Fickian at  $t = \mu$ ,  $\sigma_x^2/2t$  is not yet an accurate approximation. For this particular run, the experimentally determined dispersion coefficient underestimates the final Fickian value by 14%.

$\langle D_z \rangle / u_{*H} H = 0.073$ , which is comparable to the value  $\langle D_z \rangle / u_{*H} H = 0.067$  for logarithmic boundary layers [Fischer *et al.*, 1979, p. 93]. Therefore the vertical mixing rates are comparable, such that the difference in  $K_x$  must be attributed to the difference in the velocity variance. From equation (2), the contribution of velocity heterogeneity to dispersion can be isolated in the expression

$$I = -\frac{1}{H} \int_0^H u'' \int_0^z u'' dz dz \sim u_{*H}^2 H^2 \quad (29)$$

For logarithmic layers,  $I_{bl} = 0.46 u_{*H}^2 H^2$ . For a representative vegetated channel, we consider the two-layer velocity profile shown in Figure 1, with layers of equal depth, i.e.,  $h = H/2$ . The velocities  $U_2$  and  $U_1$  are uniform across the respective layers. For this vegetated-channel profile,

$$I_{vc} = \frac{1}{48} (U_2 - U_1)^2 H^2 \quad (30)$$

[after Fischer *et al.*, 1979, p. 93]. Data from Table 1 implies that  $(U_2 - U_1) = (3.1 \pm 0.7) u_{*H}$ . Substituting into equation (30) yields  $I_{vc} = 0.20 u_{*H}^2 H^2$  for a vegetated channel. Thus,  $I_{bl}/I_{vc} = 2.4$ . This indicates that for a fixed potential gradient, i.e., fixed  $u_{*H} = \sqrt{gSH}$ , the bare channel has more than twice the velocity heterogeneity, explaining why the dispersion is nearly twice as high. The greater velocity heterogeneity is simply due to the greater mean velocity that is possible in the low resistance open channel compared to the high resistance vegetated channel.

[29] Now we consider the regime of wake-diffusion dominated exchange (i.e.,  $C_D a h > 2$ , as discussed in section 2.2). We will examine equation (18) for typical field conditions. Because our experimental conditions

could not be extended into this regime, equation (18) has not been experimentally verified, and this section should be treated as hypothesis. The highest vegetation density observed in the field corresponds to  $ad = 0.4$  (mangrove, Mazda *et al.* [1997]). Since vortex-driven exchange is expected to dominate in sparse canopies ( $ad < 0.1$ ), here we consider a range  $0.1 < ad < 0.4$ . We use the constant aspect ratio,  $d/h = 0.05$ , based on geometric similitude observed among aquatic plants [Niklas, 1994]. It is also reasonable to assume  $C_D = 1$ . Data from the vortex-driven exchange regime (Table 1) implies that  $(U_2 - U_1)/u_{*H} = 3.07 \pm 0.69$  and we use this as an approximation for the case of diffusion-dominated exchange. The resulting nondimensional dispersion coefficients for  $ad =$

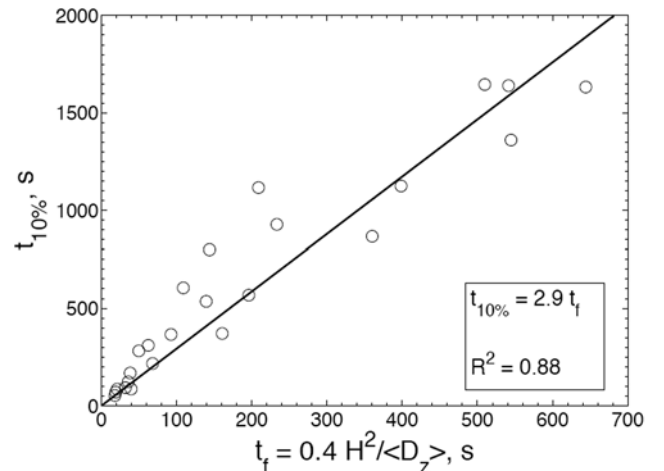


**Figure 9.** Regression analysis between  $t_{10\%}$  and the Fickian timescale,  $t_f = 0.4 H^2 / \langle D_z \rangle$ .

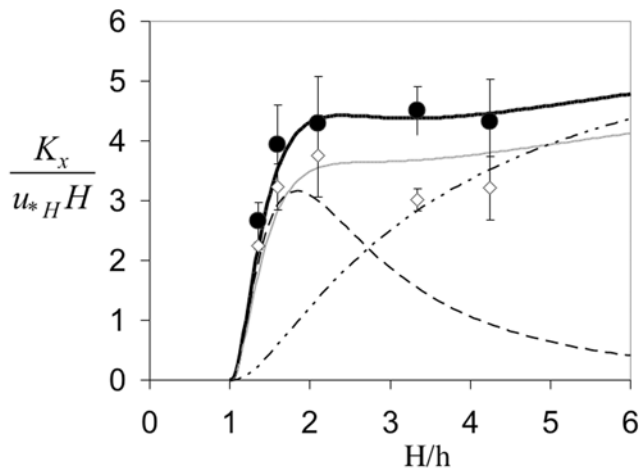


**Figure 10.** Experimentally measured coefficients of dispersion,  $K_x$ , normalized by  $u_{*H}H$  and then ensemble-averaged for each value of  $H/h$ . Diamonds are raw data and circles are adjusted with the RWPT model. The gray line is equation (12) with  $\beta = 110$  and  $\gamma = 5.9$ . A least squares fit (heavy black line) of equation (12) to the corrected observations yields  $\beta = 140$  and  $\gamma = 6.9$ . For this case the contributions of the first (dash line) and second (dash dot line) terms in equation (4) are shown.

0.1 and  $ad = 0.4$  are shown in Figure 13. The dimensionless dispersion is an order of magnitude higher with diffusion-limited-exchange than with the vortex-driven-exchange (Figures 10 and 13). This is expected because the slower exchange rate in the diffusion-limited regime produces longer retention time in the vegetation, and therefore, a larger dispersion. However, it takes much longer for this dispersive regime to develop and to reach its Fickian limit. The exchange term also remains dominant

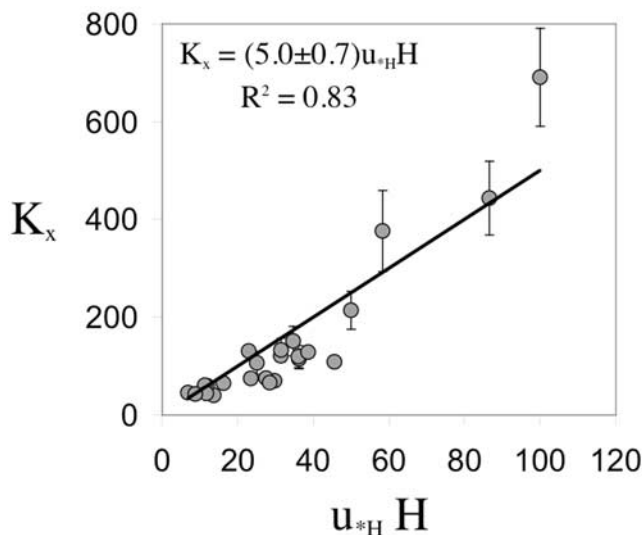


**Figure 11.** Least squares linear fit of the adjusted experimental data to depth-scale shear parameter,  $u_{*H}H$ . Vertical lines represent experimental uncertainty. The correlation is significant ( $R^2 = 0.83$ ,  $n = 24$ ).

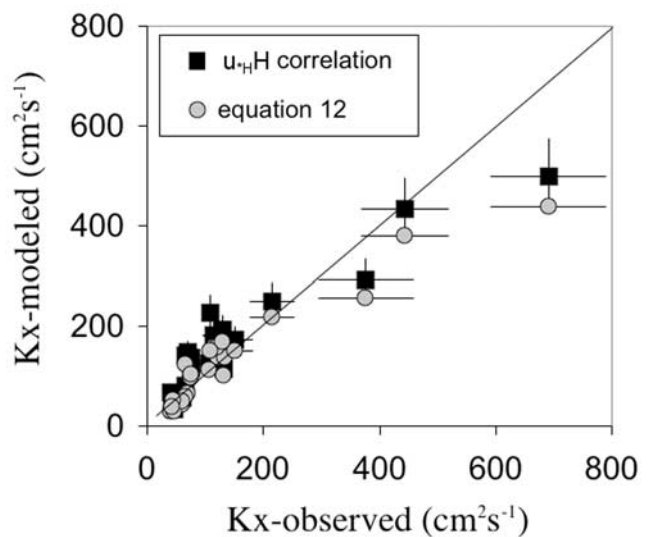


**Figure 12.** Modeled and observed  $K_x$ . Circles represent equation (12) with  $\beta = 140$  and  $\gamma = 6.9$ . The agreement between the model and observations is highly significant,  $R^2 = 0.81$ ,  $n = 24$ . Squares represent the  $u_{*H}H$  correlation determined in Figure 11. This agreement is less significant, with  $R^2 = 0.72$ ,  $n = 24$ . Horizontal bars represent experimental uncertainty. Vertical bars represent uncertainty in model coefficients.

to higher values of  $H/h$  than in the vortex-driven-exchange, with shear-dispersion becoming dominant only after  $H/h = 6$ .

[30] Although the model developed in this paper was experimental tested with a rigid canopy, the model framework applies to flexible and even waving canopies. One needs only to determine the coefficients  $\beta_1$ ,  $\beta_2$ , and  $b$ . Some insight can be gained from the study of Ghisalberti and Nepf [2006] (for example, see their Figure 6), who show that the ratio  $u_*/\Delta U$  decreases as the movement of the canopy increases, i.e., exchange of momentum between the

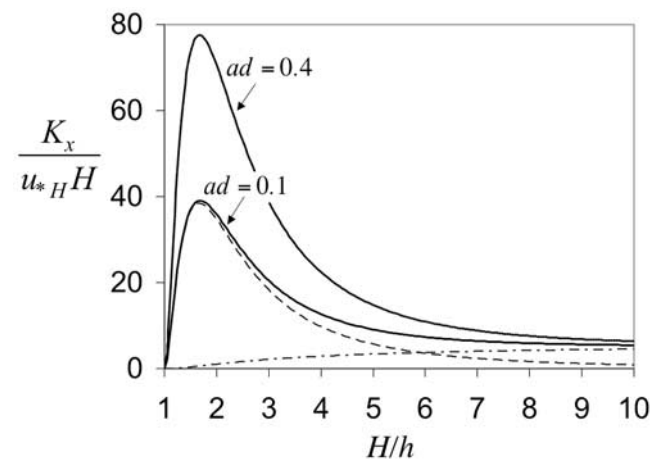


**Figure 13.** Nondimensional dispersion in the regime of diffusion-driven exchange, from equation (18), for typical field conditions:  $d/h = 0.05$ ,  $C_D = 1$ , and  $ad = (0.1, 0.4)$  shown as solid lines. For the case  $ad = 0.1$  the individual contributions of diffusion-limited exchange (dashed) and fast-zone shear dispersion (dash-dot) are also shown.

slow (canopy) zone and the fast (overflow) zone becomes less efficient. Their observations indicate that  $\beta_2 = \Delta U/u_*$  increases with canopy flexibility/motion, and imply, through the transport analogy, that the mass exchange coefficient  $b$  will decrease as canopy flexibility/motion increases.

## 5. Conclusion

[31] A theoretical framework has been proposed for evaluating the longitudinal dispersion coefficient in channels with submerged vegetation. The two-zone model identifies three contributing processes: large-scale shear dispersion above the canopy, inefficient exchange between the canopy and the overflow, and stem-scale dispersion within the canopy. For shallow relative submergence ( $H/h < 3$ ), the inefficient exchange dominates the total dispersion. As  $H/h$  increases, large-scale shear dispersion eventually dominates, and, as expected, approaches the limit for logarithmic boundary layers for  $H/h \rightarrow \infty$ . For sparse canopies ( $C_D ah$  small), exchange between the canopy and overflow is governed by K-H vortices, and for dense canopies ( $C_D ah$  large), this exchange is governed by in-canopy turbulent diffusion. In the latter case the exchange is much slower, and the resulting dispersion coefficients are much greater. Finally, we suggest that the single-point estimator  $K_x = \sigma_x^2/2t$  is reasonable, but only after a time-since-release of  $t > 2.9t_f$ , where  $t_f = H^2/|<D_z>$ .

## Notation

$a$ (cm <sup>-1</sup> )	Frontal area per volume
$b$ (cm s <sup>-1</sup> )	Canopy exchange coefficient
$C_D$	Drag coefficient
$C$ (g cm <sup>-3</sup> )	Concentration
$d$ (cm)	Stem diameter
$D_w$ (cm <sup>2</sup> s <sup>-1</sup> )	Vertical diffusivity in wake zone
$D_z$ (cm <sup>2</sup> s <sup>-1</sup> )	Vertical diffusivity
$h$ (cm)	Canopy height
$H$ (cm)	Water depth
$K_x$ (cm <sup>2</sup> s <sup>-1</sup> )	Total dispersion coefficient
$K_i$ (cm <sup>2</sup> s <sup>-1</sup> )	Dispersion coefficient in $i$ th zone
$M_i$	$i$ th temporal moment
$t$ (s)	Time
$T$ (s)	Full-depth transport timescale
$U_i$ (cm s <sup>-1</sup> )	Velocity in $i$ th zone
$\Delta U$ (cm s <sup>-1</sup> )	Velocity difference across shear layer
$u_*$ (cm s <sup>-1</sup> )	$\sqrt{gS(H-h)}$
$u_{*H}$ (cm s <sup>-1</sup> )	$\sqrt{gSH}$
$U_c$ (cm s <sup>-1</sup> )	Center of mass velocity
$X$ (cm)	Distance from injection to probe
$z_1$ (cm)	Interface between wake and exchange zones
$\beta_1$	$(U_2 - U_1)/\Delta U$
$\beta_2$	$\Delta U/u_*$
$\beta$	$40\beta_1\beta_2$
$\gamma$	Shear dispersion scale coefficient
$\sigma_i$ (s)	Standard deviation of $i = x$ or $t$
$\mu$ (s)	Center of mass arrival time
$\nu$ (cm <sup>2</sup> s <sup>-1</sup> )	Kinematic viscosity

[32] **Acknowledgments.** This material is based upon work supported by the National Science Foundation under grant EAR-0309188. Any opinions, findings, or recommendations expressed in this material are those of the author(s) and do not necessarily reflect the views of the National Science Foundation. The first author was supported in part by a Fulbright/Marine Institute Scholarship (2004–2005). The authors wish to thank Peter Israelsson for his comments on the particle-tracking model and Lindsey Sheehan for her help in the laboratory.

## References

- Aris, R. (1956), On the dispersion of a solute in a fluid flowing through a tube, *Proc. R. Soc. Lond.*, *A235*, 67–77.
- Carollo, F., V. Ferro, and D. Termini (2002), Flow velocity measurements in vegetated channels, *J. Hydraul. Eng.*, *128*(7), 664–673.
- Chikwendu, S. (1986), Calculation of longitudinal shear dispersivity using an N-zone model as  $N \rightarrow \infty$ , *J. Fluid Mech.*, *167*, 19–30.
- Chikwendu, S., and G. Ojiakor (1985), Slow-zone model for longitudinal dispersion in two-dimensional shear flows, *J. Fluid Mech.*, *152*, 15–38.
- Davis, P., T. Atkinson, and T. Wigley (2000), Longitudinal dispersion in natural channels: 2. The roles of shear flow dispersion and dead zones in the River Severn, U.K., *Hydrol. Earth Syst. Sci.*, *4*(3), 355–371.
- Day, T. (1975), Longitudinal dispersion in natural channels, *Water Resour. Res.*, *11*(6), 909–918.
- Elder, J. (1959), The dispersion of marked fluid in turbulent shear flow, *J. Fluid Mech.*, *5*, 544–560.
- Fischer, H. (1973), Longitudinal dispersion and turbulent mixing in open-channel flow, *Annu. Rev. Fluid Mech.*, *5*, 59–78.
- Fischer, H., E. List, R. Koh, J. Imberger, and N. Brooks (1979), *Mixing in Inland and Coastal Waters*[BT], 483 pp., Elsevier, New York.
- Ghisalberti, M., and H. Nepf (2002), Mixing layers and coherent structures in vegetated aquatic flows, *J. Geophys. Res.*, *107*(C2), 3011, doi:10.1029/2001JC000871.
- Ghisalberti, M., and H. Nepf (2004), The limited growth of vegetated shear layers, *Water Resour. Res.*, *40*, W07502, doi:10.1029/2003WR002776.
- Ghisalberti, M., and H. Nepf (2005), Mass transport in vegetated shear flows, *Environ. Fluid Mech.*, *5*(6), 527–551.
- Ghisalberti, M., and H. Nepf (2006), The structure of the shear layer over rigid and flexible canopies, *Environ. Fluid Mech.*, *6*(3), 277–301, doi:10.1007/s10652-006-0002-4.
- Hoteit, H., R. Mose, A. Younes, F. Lehmann, and P. Ackerer (2002), Three-dimensional modeling of mass transfer in porous media using the mixed hybrid finite elements and the random-walk methods, *Math. Geol.*, *34*(4), 435–456.
- Ikeda, S., and M. Kanazawa (1996), Three-dimensional organized vortices above flexible water plants, *J. Hydraul. Eng.*, *122*(11), 634–640.
- Kadlec, R., and R. Knight (1996), *Treatment Wetlands*, 893 pp., Lewis Publishers, Boca Raton, FL.
- Kouwen, N., T. Unny, and H. Hill (1969), Flow retardance in vegetated channels, *J. Irrig. Drain. Div. ASCE*, *95*(2), 329–342.
- Leland, H. (2003), The influence of water depth and flow regime on phytoplankton biomass and community structure in a shallow, lowland river, *Hydrobiologia*, *506-509*, 247–255.
- Leonard, L., and M. Luther (1995), Flow hydrodynamics in tidal marsh canopies, *Limnol. Oceanogr.*, *40*(8), 1474–1484.
- Leonard, L., and D. Reed (2002), Hydrodynamics and sediment transport through tidal marsh canopies, *J. Coast. Res.*, *SI36*, 459–469.
- Levenspiel, O., and W. K. Smith (1957), Notes on the diffusion-type model for the longitudinal mixing of fluids in flow, *Chem. Eng. Sci.*, *6*, 227–233.
- Lightbody, A., and H. Nepf (2006), Prediction of velocity profiles and longitudinal dispersion in emergent salt marsh vegetation, *Limnol. Oceanogr.*, *51*(1), 218–228.
- Lopez, F., and M. Garcia (1998), Open-channel flow through simulated vegetation: Suspended sediment transport modeling, *Water Resour. Res.*, *34*(9), 2341–2352.
- Lopez, F., and M. Garcia (2001), Mean flow and turbulence structure of open-channel flow through non-emergent vegetation, *J. Hydraul. Eng.*, *127*(5), 392–402.
- Mars, M., M. Kuruvilla, and H. Goen (1999), The role of the submergent macrophyte *Triglochin huegelii* in domestic greywater treatment, *Ecol. Eng.*, *12*, 57–66.
- Mazda, Y., E. Wolanski, B. King, A. Sase, D. Ohtsuka, and M. Magi (1997), Drag force due to vegetation in mangrove swamps, *Mangroves Salt Marshes*, *1*, 193–199.
- Murphy, E. (2006), *Dispersion in flow with submerged canopies*, M.S. thesis, Massachusetts Institute of Technology, Cambridge, Massachusetts.

- Nepf, H. (1999), Drag, turbulence, and diffusion in flow through emergent vegetation, *Water Resour. Res.*, 35(2), 479–489.
- Nepf, H., and E. Vivoni (2000), Flow structure in depth-limited, vegetated flow, *J. Geophys. Res.*, 105(C12), 28,547–28,557.
- Nepf, H., C. Mugnier, and R. Zavistoski (1997a), The effects of vegetation on longitudinal dispersion, *Estuar. Coast. Shelf Sci.*, 44, 675–684.
- Nepf, H., J. Sullivan, and R. Zavistoski (1997b), A model for diffusion within emergent vegetation, *Limnol. Oceanogr.*, 42(8), 1735–1745.
- Nepf, H., M. Ghisalberti, B. White, and E. Murphy (2007), Retention time and dispersion associated with submerged aquatic canopies, *Water Resour. Res.*, 43, W04422, doi:10.1029/2006WR005362.
- Niklas, K. (1994), The scaling of plant and animal body mass, length, and diameter, *Evolution*, 48(1), 44–54.
- Nordin, C., and B. Troutman (1980), Longitudinal dispersion in rivers: The persistence of skewness in observed data, *Water Resour. Res.*, 16(1), 123–128.
- Oldham, C., and J. Sturman (2001), The effect of emergent vegetation on convective flushing in shallow wetlands: Scaling and experiments, *Limnol. Oceanogr.*, 46(6), 1486–1493.
- Palmer, M., H. Nepf, T. Petterson, and J. Ackerman (2004), Observations of particle capture on a cylindrical collector: Implications for particle accumulation and removal in aquatic systems, *Limnol. Oceanogr.*, 49, 76–85.
- Poggi, D., A. Porporato, L. Ridol, J. Albertson, and G. Katul (2004), The effect of vegetation density on canopy sub-layer turbulence, *Bound. Layer Meteorol.*, 111, 565–587.
- Raupach, M., J. Finnigan, and Y. Brunet (1996), Coherent eddies and turbulence in vegetation canopies: The mixing-layer analogy, *Bound. Layer Meteorol.*, 78, 351–382.
- Roberts, A., and D. Strunin (2004), Two-zone model of shear dispersion in a channel using centre manifolds, *Q. J. Mech. Appl. Math.*, 57(3).
- Ross, O., and J. Sharples (2004), Recipe for 1-D Lagrangian particle tracking models in space-varying diffusivity, *Limnol. Oceanogr. Methods*, 2, 289–302.
- Schultz, M., H.-P. Kozerski, T. Pluntke, and K. Rinke (2002), The influence of macrophytes on sedimentation and nutrient retention in the lower River Spree, *Water Res.*, 37, 569–578.
- Smith, R. (1981), A delay-diffusion description for contaminant dispersion, *J. Fluid Mech.*, 105, 469–486.
- Stephan, U., and D. Gutknecht (2002), Hydraulic resistance of submerged flexible vegetation, *J. Hydrol.*, 269, 27–43.
- Stone, B., and H. Shen (2002), Hydraulic resistance of flow in channels with cylindrical roughness, *J. Hydraul. Eng.*, 128(5), 500–506.
- Thacker, W. C. (1975), A solvable model of “shear dispersion”, *J. Phys. Oceanogr.*, 6, 66–75.
- Thomson, D., W. Physick, and R. Maryon (1997), Treatment of interfaces in random walk dispersion models, *J. Appl. Meteorol.*, 36, 1284–1295.
- Valentine, E., and I. Wood (1977), Longitudinal dispersion with dead zones, *J. Hydraul. Div. A.S.C.E.*, 103, 975–990.
- van Masijk, A., and E. Veling (2005), Tracer experiments in the Rhine Basin: Evaluation of the skewness of observed concentration distributions, *J. Hydrol.*, 307, 60–78.
- White, B., and H. Nepf (2003), Scalar transport in random cylinder arrays at moderate Reynolds number, *J. Fluid Mech.*, 487, 43–79.
- White, B., M. Ghisalberti, and H. Nepf (2003), Shear layers in partially vegetated channels: Analogy to shallow water shear layers, in *Shallow Flows*, edited by G. Jirka and W. Uijtewaal, pp. 267–273, A. A. Balkema, Brookfield, Vt.
- White, F. (1974), *Viscous Fluid Flow*, 725 pp., McGraw-Hill, New York, NY.
- Wilensky, U. (1999), Netlogo, *Tech. Rep.*, Center for Connected Learning and Computer-Based Modeling, North-Western University, Evanston, Illin.

---

M. Ghisalberti, School of Environmental Systems Engineering, University of Western Australia, Crawley, Western Australia, Australia.

E. Murphy and H. Nepf, Department of Civil and Environmental Engineering, Massachusetts Institute of Technology, Cambridge, MA, USA. (hmnepf@mit.edu)